Measurement of the electric quadrupole amplitude within the 1283-nm $6P_{1/2}$-$6P_{3/2}$ transition in atomic thallium

P. K. Majumder and Leo L. Tsai*
Department of Physics, Williams College, Williamstown, Massachusetts 01267
(Received 4 January 1999)

We have measured the ratio of the electric quadrupole ($E2$) to magnetic dipole ($M1$) transition amplitude within the $6P_{1/2} \rightarrow 6P_{3/2}$ transition in atomic thallium. Defining χ to be this $E2$ to $M1$ amplitude ratio, we find that $\chi = 0.2387(10)(38)$, where the first error is statistical and the second represents a combined systematic error. In addition to providing a stringent test of theoretical wave-function calculations in thallium, accurate knowledge of this quantity is essential for existing and future measurements of parity nonconserving optical rotation on this same 1283-nm line in thallium. [S1050-2947(99)07307-2]

PACS number(s): 32.70.Cs, 32.80.Ys

I. INTRODUCTION

Measurements of atomic parity nonconservation (PNC) have now reached the level of precision required to provide important tests of the electroweak standard model. All such tests also require atomic structure calculations of comparable precision from which one can extract the electroweak quantity of interest, Q_w, the ''weak charge,'' from the experimental atomic observable. For the case of cesium, a recent precision measurement of PNC [1] coupled with a highly accurate calculation [2] has placed stringent new constraints on possible extensions to the standard model [1,3]. In thallium, a PNC measurement of 1% accuracy [4], coupled with an existing 3% atomic theory calculation [5], yields a second atomic test of electroweak physics. Improved accuracy is expected from new thallium PNC calculations now underway [6]. To test the accuracy and guide the refinement of these calculations, independent thallium atomic structure measurements of comparable accuracy are required. Except for hyperfine structure measurements in the lowest-lying states [7], such precise experimental data have not been available for this element.

This paper describes the results of the first of a series of planned precision measurements in thallium. In a vapor cell laser-polarimetry apparatus, we have measured χ, the ratio of electric quadrupole ($E2$) to dominant magnetic dipole ($M1$) amplitude, within the 1283 nm $6P_{1/2}$-$6P_{3/2}$ transition in thallium. As the $M1$ amplitude can be calculated to very high precision *without* the need for precise wave functions, this measurement yields a value for the $E2$ matrix element and hence provides a direct test of the wave-function accuracy of the relevant thallium states. In addition, χ is a line-shape parameter whose accurate knowledge is essential for determination of the PNC observable in atomic experiments such as those recently performed on this transition by the groups in Seattle [4] and in Oxford [8]. Presently, a 2.2σ (7%) discrepancy exists between the two measurements. The result of the measurement of χ reported here differs significantly from an older theoretical estimate of this quantity, which was assumed in the analysis of the PNC observable in [8]. On the other hand, an experimental determination of χ made during the course of the Seattle experiment [4] [9] is in excellent agreement with our new value. At the end of this paper we briefly consider the results of line-shape simulations which quantify the correlation between χ and the extracted value of the PNC observable. Finally, possible future PNC work of improved precision on this transition [10] would require as input a highly precise, independent measurement of χ such as we report here.

II. DETAILS OF THE EXPERIMENT

Figure 1 shows the details of the energy-level structure for the 1283-nm transition in thallium. The two stable isotopes, ^{203}Tl and ^{205}Tl, each have nuclear spin $I = \frac{1}{2}$, and exhibit a small ($\sim$100 MHz) isotopic shift for this particular transition. Neither this shift nor the splitting between the $F' = 1$ and $F' = 2$ excited state hyperfine levels is spectrally resolved in our experiment, due to Doppler broadening. The large 21 GHz splitting of the $6P_{1/2}$ ground state $F = 0$ and $F = 1$ hyperfine levels allows us to study independently two ''groups'' of four constituent lines. Consideration of selection rules shows that while the $F = 0 \rightarrow F' = 1$ and $F = 0 \rightarrow F' = 2$ transitions are purely $M1$ and purely $E2$ in char-

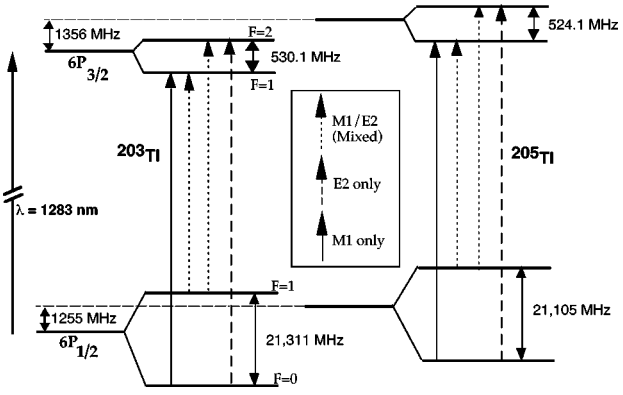

FIG. 1. The 1283-nm $6P_{1/2} \rightarrow 6P_{3/2}$ transition in atomic thallium, showing hyperfine splitting, isotopic shifts (not to scale), as well as component magnetic dipole and electric quadrupole transitions.

*Present address: Emmanuel College, Cambridge University, Cambridge, CB2 3AP, United Kingdom.

 ©1999 The American Physical Society

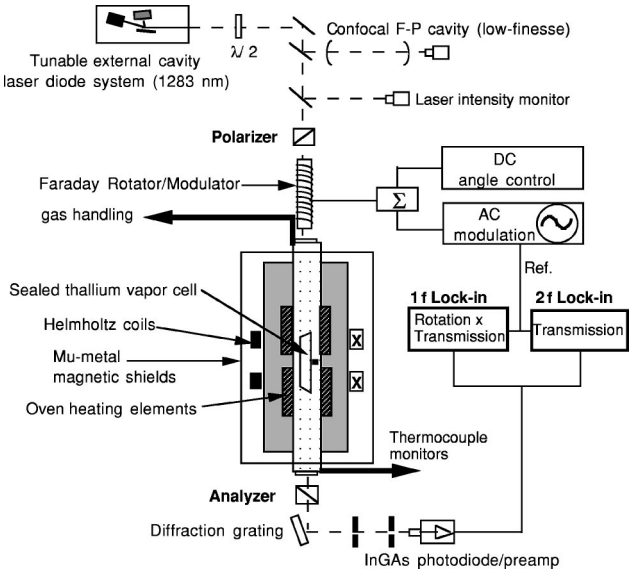

FIG. 2. Schematic diagram of the experimental setup (see text).

acter, respectively, transitions originating from $F=1$ are of a mixed $E2$ and $M1$ character. Despite the absence of resolved spectral structure, we are able to extract precise and reliable values for the electric quadrupole to magnetic dipole amplitude ratio for a number of reasons. First, all excited state hyperfine splittings, isotopic shifts, and abundances are very well known [7] and can be included in line-shape models. Second, the very high signal-to-noise ratio of our spectra allows us to optimize simultaneously the line-shape parameter for χ along with optical depth and spectral linewidth parameters within our fitting procedure. Finally, we can analyze a wide range of distinct line shapes, corresponding to different ground-state hyperfine levels, Faraday optical rotation versus transmission spectra, and low versus high optical depth scans, each having distinctly different dependence on the parameter χ. Use of a sealed, evacuated vapor cell in this experiment creates an interaction region which is spatially limited to a region of uniform temperature, and at the same time lacks buffer gas collisions. This minimizes any potential complications to the experimental line shapes introduced by extended, buffer gas-confined interaction regions which characterize the PNC optical rotation setups optimized to achieve maximum optical depth.

The method of simultaneous detection of transmission and Faraday rotation line shapes is similar to that used in recent PNC optical rotation experiments in thallium and lead [4,11]. Referring to Fig. 2, roughly 10 mW of 1283 nm light is generated by an external cavity diode laser whose residual short-term frequency jitter was measured to be 2–3 MHz. A small fraction of the light is directed into a confocal Fabry-Perot cavity for frequency calibration, as well as a photodiode for intensity normalization. The laser light then passes through a calcite polarizer and a Faraday rotator. The rotator consists of a Faraday glass rod to which we apply a combination of ac and dc magnetic fields. Using this device, we modulate the laser polarization sinusoidally by several milliradians at a frequency of 700 Hz. The light is then incident on the 20-cm-long sealed quartz vapor cell containing roughly 5 g of thallium. The cell is contained within an evacuated 48-in. ceramic tube whose central region is externally heated via ac current applied to two pairs of clamshell heaters. Entrance and exit windows of the ceramic tube extend well beyond the heated region of the oven. A variable duty-cycle heater control circuit maintains cell temperatures of up to 950 °C with a long-term stability of better than 1 °C. The cell temperature was directly monitored using thermocouples located at the cell stem and one cell window and was displayed and recorded with $\pm 1°$ accuracy by a multiple-channel thermocouple monitor (Stanford Research Systems, SR630). A pair of Helmholtz coils located inside Mumetal magnetic shields produce longitudinal magnetic fields of up to 100 mG to allow measurement of Faraday optical rotation. The longitudinal shielding factor offered by the Mumetal (roughly 100) was sufficient to reduce optical rotation noise due to residual magnetic field fluctuations to an insignificant level. Since the observed Faraday rotation amplitude depends only on the integrated longitudinal field along the interaction region, residual nonuniformity in longitudinal field did not lead to complications in the analysis of experimental rotation spectra [12].

After passing through a (nearly crossed) analyzer prism, the laser light is spatially filtered via a diffraction grating and collimators. In this way the signal reaching the InGaAs PIN photodiode detector is nearly free of infrared oven blackbody light. The amplified detector signal is sent to two digital lock-in amplifiers set to detect frequency components of the transmitted laser intensity at the fundamental and second harmonic modulation frequencies, respectively. As explained in detail in [11], the second-harmonic signal is proportional to the laser transmission, while the signal at the fundamental frequency is proportional to the product of transmission times optical rotation. Since these signals are obtained simultaneously, the former signal can be analyzed independently to provide transmission spectrum information, allowing pure optical rotation information to be extracted from the latter.

Using this setup we are able to achieve an optical rotation resolution of approximately 2×10^{-7} rad/$\sqrt{\text{Hz}}$, as compared to the typical 10^{-3} rad amplitude of our Faraday rotation signals. Data were taken using temperatures in the range of 850 °–950 °C, which correspond to optical depths ranging from 0.5–4.0 with our vapor cell. A typical data run consists of two pairs of up-down frequency sweeps. By switching off the longitudinal magnetic field for one of the two sweeps, and subtracting the optical rotation signals, we remove a small background signal from our Faraday rotation line shape. The background pattern, whose typical size was two orders of magnitude smaller than the Faraday signal, originates from frequency-dependent optical transmission changes (unrelated to the atoms) which are indistinguishable from a true optical rotation in our apparatus. We acquired data in a ''field on-off-off-on'' pattern in order to study the possibility of a slow drift in the background pattern. Over the 1 min time scale of the subtraction, no significant drift was observed. Data were obtained for the $F=0$ and $F=1$ hyperfine groups separately, yielding a total of four distinct line-shapes which could be analyzed.

III. LINE-SHAPE ANALYSIS AND EXPERIMENTAL RESULTS

The general form of the transmission for a given ground-state hyperfine level, i, is $T_i(\nu)=I_0\exp[-A_i(\nu)]$, where

$A_i(\nu)$ is the composite absorption line shape. As discussed, for this transition, there exist magnetic dipole and electric quadrupole contributions to the absorptivity. We express the absorption spectrum as

$$A_i(\nu)\propto(Nl)\langle M1\rangle^2\sum_{j=1}^{2}\sum_{k=1}^{2}a_k[K_{ij}^{(1)}+\chi^2K_{ij}^{(2)}]\times\mathcal{V}(\nu-\nu_{ijk};\gamma,\Gamma). \quad (1)$$

We define $\langle M1\rangle$ as the reduced magnetic dipole matrix element, $\langle J_e||\mu||J_g\rangle$, where $J_g=\frac{1}{2}$ and $J_e=\frac{3}{2}$, referring to the ground and excited states, respectively. Here, N and l refer to the number density of atoms and the length of the cell, which together with $\langle M1\rangle^2$ determine the observed optical depth. The first and second summation refer to excited state hyperfine level and isotope, respectively, with the coefficient a_k accounting for isotopic abundance. The $K^{(a)}$ coefficients in Eq. (1) account for relative line-strength differences among the magnetic dipole ($a=1$) and electric quadrupole ($a=2$) hyperfine components of the overall transition probability,

$$K_{ij}^{(a)}=\frac{(2F_i+1)(2F_j+1)}{2a+1}\begin{Bmatrix}J_g & a & J_e\\ F_j & I & F_i\end{Bmatrix}^2, \quad (2)$$

where the bracketed term represents a $6j$ symbol. In Eq. (1), $\mathcal{V}$ is the normalized Voigt profile line shape determined by the component collisional and Doppler widths, γ and Γ, respectively, and ν_{ijk} is the resonance frequency of a particular hyperfine transition of a specific isotope. Given the particular form of $A_i(\nu)$ above, we quote the following precise definition for χ:

$$\chi\equiv\frac{\omega}{4\sqrt{3}}\frac{\langle J_e||Q^{(2)}||J_g\rangle}{\langle J_e||\mu||J_g\rangle}, \quad (3)$$

where the term containing $Q^{(2)}$ is the reduced matrix element of the electric quadrupole operator. Using the derivation in [13], one can equivalently express χ in terms of the Einstein A coefficients for spontaneous magnetic dipole and electric quadrupole decay, A_{M1} and A_{E2}, from the $6P_{3/2}$ excited state: $\chi\equiv\sqrt{5A_{E2}/3A_{M1}}$.

The Faraday rotation line shape $\Phi^F(\nu)$ arises from a Zeeman frequency shift in a longitudinal magnetic field, B_0, which leads to a frequency-dependent change in the real part of the refractive index for circular polarization components of the light. When the Zeeman splitting is small compared to the linewidth, there results an optical rotation of plane-polarized light whose line shape follows the derivative of the dispersion curve. We can write

$$\Phi^F{}_i(\nu)\propto(Nl)\langle M1\rangle^2B_0\sum_{j=1}^{2}\sum_{k=1}^{2}\times a_k[U_{ij}^{(11)}+2\chi U_{ij}^{(12)}+\chi^2U_{ij}^{(22)}]\mathcal{D}'(\nu-\nu_{ijk};\gamma,\Gamma). \quad (4)$$

The U_{ij} factors are proportional to $6j$ symbols as well as appropriate g factors characterizing the Zeeman splitting. The superscripts on these factors reflect the tensor origin of the relevant transition matrix elements. Analytic expressions for these factors are quite involved, and can be found, for example, in [14]. For the case of the $F=1$ ground-state transitions, the Faraday rotation line shape is characterized by terms linear in χ due to the interference of allowed $M1$ and $E2$ amplitudes (i.e., $U_{1j}^{(12)}\neq0$). This dependence on χ is quite distinct from either the $F=0$ Faraday rotation line shape or the absorption line shapes which depend on this quantity only quadratically. In this small-field limit, the magnitude of the Faraday rotation scales with both the optical depth and the magnetic field amplitude. $\mathcal{D}'(\nu)$ is the symmetric line shape corresponding to the derivative of the normalized dispersion curve. A small additional component in the observed Faraday rotation due to state mixing in the magnetic field (and therefore to the dispersion line shape itself) is also taken into account [14]. Our nonlinear least-squares-fitting routine incorporates these relative line strength factors as well as isotopic shifts and hyperfine splitting information to create theoretical line shapes for the analysis of experimental spectra.

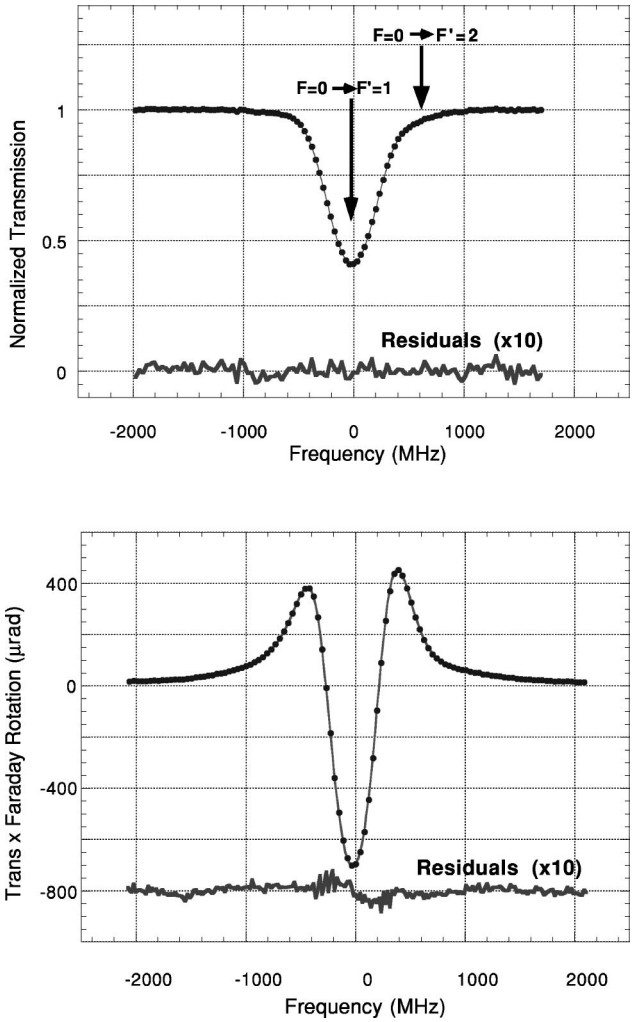

FIG. 3. Transmission and (Faraday rotation × transmission) line shapes for the $F=0$ ground-state hyperfine group showing data (dots) and fitted curve (line). Unresolved excited-state hyperfine structure is highlighted by the arrows in the transmission spectrum. Shown below, expanded by a factor of 10, are the residuals of the fits. The data shown require less than 1 min to acquire.

Figures 3 and 4 show data and corresponding fits of an individual transmission and background-subtracted Faraday

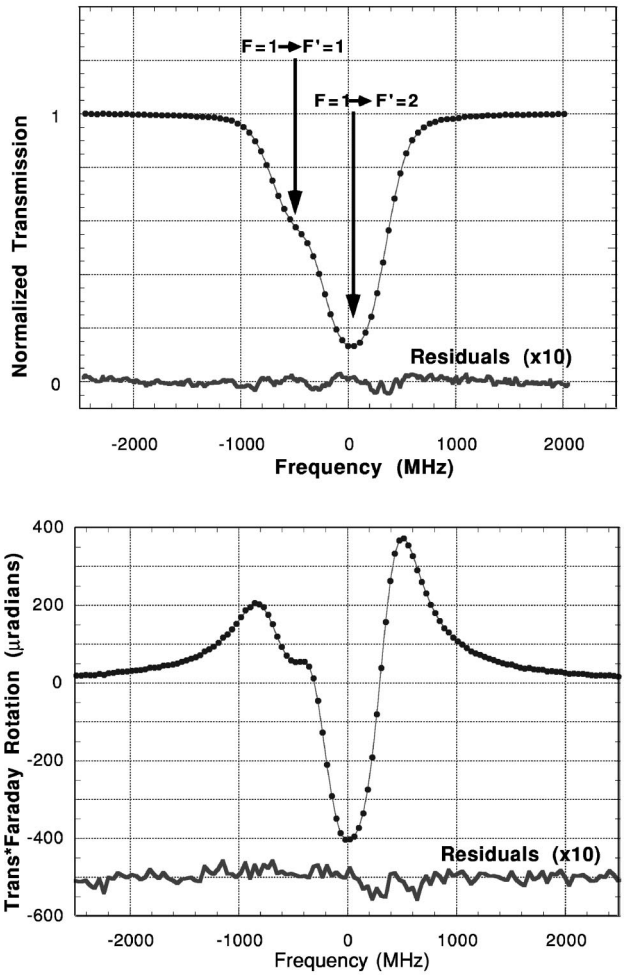

FIG. 4. Transmission and (Faraday rotation × transmission) line shapes for the $F=1$ ground-state hyperfine group showing data (dots) and fitted curve (line). Shown below, expanded by a factor of 10, are the residuals of the fits.

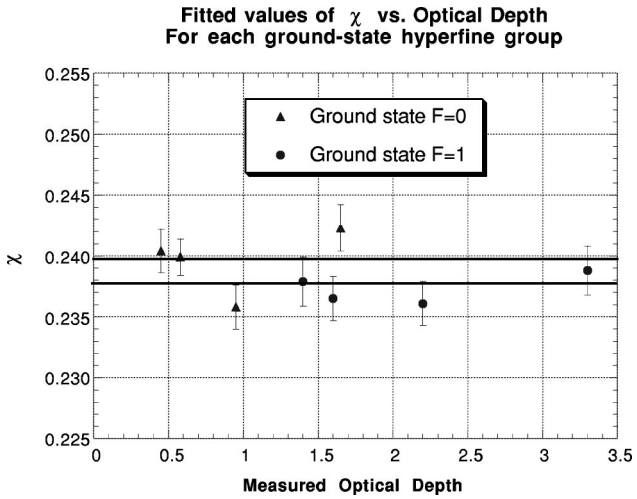

FIG. 5. Results of fitted values for χ binned according to measured optical depth. Ground-state $F=0$ and $F=1$ fit results are shown separately. Fit results from upward- and downward-going laser sweeps, as well as from transmission and Faraday rotation scans, were averaged prior to binning. Horizontal lines indicate ± 1 standard deviation statistical errors only.

rotation scan for each of the ground-state hyperfine groups. As a first step in the analysis, the laser frequency sweep was calibrated and linearized using information obtained from the Fabry-Perot transmission data. This step is essential given the hysteresis and nonlinearity associated with the PZT devices used for tuning the laser frequency. Two linearization schemes were employed. The first consisted of explicit fits of the Fabry-Perot data to an Airy function using a nonlinear (polynomial) mapping of frequency to data point number. In the second, a cubic spline interpolation of Fabry-Perot peaks was used. A comparison of the two methods showed no measurable differences in the subsequent results of atomic spectrum analysis. The ~ 540 MHz free spectral range of our confocal Fabry-Perot cavity was measured to within 0.2 MHz using a high-precision wave meter (Burleigh Instruments, model WA-1500), and this value was independently confirmed by calibration against the well-known 21 GHz thallium ground-state hyperfine splitting. Direct vapor cell temperature measurements allowed us to calculate and fix the value of the Doppler width in our data analysis. Collisions of thallium atoms in the cell result in a Lorentzian width roughly 20% as large as the Doppler width (typically 50 MHz and 250 MHz, respectively). We took explicit account of the small isotopic difference in Doppler width. The value of the Lorentzian width as well as the optical depth and χ were extracted from the fits. Data were also analyzed by allowing the Doppler width parameter to vary to study its potential effect on the fitted value of χ. We found good agreement between fitted values for the Doppler width and those predicted from cell temperature measurement. Theoretical Voigt convolution profiles were generated in the fitting program using an efficient and accurate analytic approximation technique [15] [9]. Typically, transmission line shapes were fit first, after which certain parameters, such as the fitted widths, were then fixed for subsequent fits to the (Faraday multitransmission) spectra. A typical data run yielded a value of χ with 10% statistical precision.

IV. DISCUSSION OF SYSTEMATIC ERRORS

Several hundred data runs were taken over a period of several months, with an effort made to explore as wide a range of experimental operating conditions (hyperfine group, laser sweep conditions, cell temperature) as were accessible. Figure 5 demonstrates the consistency of our results for the fitted value of χ for the two ground-state hyperfine transitions, and over a range of optical depths. The parameter χ contributes in very different ways to the various theoretical line shapes represented in this plot, making this a particularly powerful test for potential systematic errors associated with our analysis procedure.

Initial fits were performed using a ''nominal'' fitting method in which the Doppler width parameter was fixed, and the data were weighted by an experimentally-determined noise profile. This accounted for a modest increase in measured noise on the steep slopes of the line shapes due to residual laser frequency jitter. A number of other fitting strategies were implemented as well. These included a flat weighting model, as well as a model in which the wings of the measured spectra were not included in the fit. As mentioned, data were also analyzed by simultaneously floating the Doppler width parameter. Finally, we also implemented a

TABLE I. Summary of contributions to the overall systematic error in χ (see text).

Systematic error source	Uncertainty, $\Delta\chi$
Line-shape fitting method	0.0025
Frequency calibration/linearization	0.0011
Hyperfine group	0.0005
Laser sweep characteristics (direction/speed/width)	0.0018
Optical depth	0.0005
Transmission vs Faraday fits	0.0013
Combined (quadrature) total	0.0038

simultaneous χ^2 fitting procedure for transmission and associated Faraday rotation line shapes that generated common atomic fit parameters (widths, optical depth, χ). The ''composite'' fits yielded residuals which were not significantly larger than those of the individual fits, and the fitted values of the relevant parameters were in good agreement with values generated from the individual line shape analysis. The overall variation in fitted values of χ observed with the various analysis models has been distilled into a line shape-fitting systematic error, $\Delta\chi$, of 0.0025, or roughly 1%, and is the first entry in Table I above. In addition, we have explored a wide range of other potential systematic errors based on an extensive study of correlations between χ and experimental operating conditions, such as laser sweep speed and direction, and magnetic field value for Faraday fits. Table I summarizes the contributions of significant sources of systematic error among all of those which we considered. The individual $\Delta\chi$ values listed in the table are determined either by evaluating the systematic deviation resulting from the relevant reanalysis, or by determing an upper limit on the systematic error any statistically resolved correlation would produce on the value of χ itself.

Upon initial analysis, the most serious systematic error was a discrepancy between the fitted values for χ as determined independently for the transmission and Faraday fits. This effect only appeared several months after data acquisition had begun. This was eventually attributed to slow degradation of the quartz cell windows in the presence of heated thallium vapor. The resulting spurious birefringence in our polarimeter led to frequency-dependent transmission variations unrelated to the atomic absorption. This was easily seen in the fit residuals of our transmission spectrum analysis. In the nominal fitting scheme, where certain fit parameters obtained from the transmission fits were fixed during the Faraday fits, the net result of this line shape error was to produce a discrepancy between χ as obtained from the two line shapes (''χ_T'' versus ''χ_F''). We note that the alternative data analysis method whereby we simultaneously optimized fit parameters of the transmission and corresponding Faraday line shapes continued to produce values of χ in good agreement with the value obtained for earlier runs that did not show evidence for this systematic error. To confirm the origin of the systematic error, a new (unused) vapor cell was installed. Data taken in a several-week period immediately after cell replacement showed no evidence of the χ_T versus χ_F discrepancy. Ultimately, data runs subject to this systematic error were not included in the final analysis of χ, but served to set limits on the size of other potential systematic errors.

Our final result for χ is

$$\chi = 0.2387 \pm 0.0010 \pm 0.0038, \tag{5}$$

where the first error is statistical and the second represents the combined systematic error. This can be compared to a recent experimental estimate of this quantity made in the course of the Seattle group's PNC measurement [4,9] of $\chi = 0.240$. Our value differs by 7% from the long-standing theoretical value [16] of $\chi = 0.254$. We note that a more recent (unpublished) theoretical value [17] for this quantity finds $\chi = 0.2395$, in excellent agreement with our new result.

V. CONNECTION BETWEEN χ AND THALLIUM PNC

Finally, we turn to the potential implications of our measurement for thallium PNC. In contrast to the approach followed here, in the PNC data analysis one *fixes* the value of χ during the analysis of experimental spectra from which the PNC observable is determined. In that case, extracted values of line shape parameters such as component linewidths and optical depth can potentially be affected by the choice of the fixed value for χ. Of particular concern is any correlation between χ and the fit parameter corresponding to the optical depth. In a PNC optical rotation experiment [4,8], the magnitude of the observed PNC rotation, ϕ_{PNC}, is given by $\phi_{\mathrm{PNC}} = C_\phi \beta R_{\mathrm{PNC}}$, where C_ϕ is an optical rotation calibration factor, β is the measured optical depth, and R_{PNC} is the atomic PNC observable proportional to the weak charge, Q_w. Typically, the β is determined through independent analysis of transmission spectra. We have demonstrated through analysis of simulated thallium line shapes that a significant anticorrelation exists between the fit parameters representing χ and the β. The size (but not the sign) of this effect depends on the particular hyperfine group, and the value of the β itself. The experimental value for R_{PNC} extracted from the above relation thus becomes directly correlated to the assumed value of χ. To explore and quantify this, we have generated simulated transmission spectra for each hyperfine group, and for a wide range of optical depths, using as input parameters typical values of Doppler and collisional widths. Simulated line shapes were generated with a certain fixed value of χ, and subsequently fit with a model which assumed a different fixed value. As under actual experimental conditions, the Doppler width, collisional width,

and optical depth parameters were simultaneously optimized in the fit to simulated transmission spectra. Any direct error that an incorrect assumed value of χ produces in the subsequent fit to the PNC optical rotation line shape is negligible compared to the indirect effect of an inaccurate χ on the fitted optical depth, as described above.

As discussed in [4] and [9], where $\chi=0.240$ was assumed, and an independent Faraday rotation calibration was used, any systematic error due to χ inaccuracy is negligible in determining the final result, $R_{\mathrm{PNC}}=-14.71(17)\times10^{-8}$. On the other hand, for the PNC experimental analysis described in [8], the older theoretical value [16], $\chi=0.254$, was assumed and fixed [18] for the analysis which resulted in the value $R_{\mathrm{PNC}}=-15.71(45)\times10^{-8}$. Considering the experimental optical depth for which PNC data were acquired in [8], and noting that R_{PNC} represents a weighted average of the PNC rotation measured on the individual hyperfine lines, our simulations suggest that the 6% overestimate of χ results in a $2.2\pm0.5\%$ overestimate in the magnitude of R_{PNC}, where the estimated error in the correction reflects uncertainty in the value for χ itself as well as limitations in the simulation procedure. Indeed, the proposed correction to the value of R_{pnc} in [8] is smaller than the 3% overall quoted uncertainty. Nevertheless, we feel it is significant that, upon applying this correction, the discrepancy between the two measured PNC values is reduced to the level of 1.3 (combined) standard deviations. Finally, we note that both of these experimental groups have also completed PNC optical rotation experiments on the $6P_0-6P_1$1.279 μm $M1$ transition in atomic lead using nearly identical experimental setups and analysis procedure to that used for the thallium work. A significant feature of the lead spectral lineshape is the *absence* of any electric quadrupole component amplitude. For the case of lead, there is complete agreement between the two experimental PNC results [11,19].

VI. CONCLUDING REMARKS

In summary, we have completed a precision measurement of the relative strength of the electric quadrupole to magnetic dipole amplitude with the 1283 nm transition in thallium. This result will provide a stringent test of new wave-function calculations presently underway. It also has a direct bearing on existing and future measurements of atomic PNC within this transition. In particular, due to the influence which the value of this parameter has on analysis of Doppler-broadened transmission spectra, our measurement suggests a small systematic correction which, if applied, significantly improves the agreement between existing PNC measurements in thallium. Due to the presence of the $M1$ transition amplitude (whose magnitude is precisely calculable without the need for detailed wave-function knowledge), we were able to determine the electric quadrupole amplitude through a relative $E2$ to $M1$ absorptivity measurement, effectively using the $M1$ absorptivity for number density normalization. This normalization feature will be employed again in a new experiment which will make use of a thallium atomic beam apparatus which has recently been constructed in our laboratory. Here the Stark-induced amplitude within the $6P_{1/2}-6P_{3/2}$ transition will be determined through measurement of the fractional change in atomic beam absorptivity at 1283 nm upon application of a large, precisely known electric field.

ACKNOWLEDGMENTS

We would like to acknowledge the valuable experimental contributions of Paul Boerner, Kyle Downey, and Peter Nicholas at various stages of this work. We thank Bruce Warrington and Kevin Jones for very helpful comments, and Nick Edwards for valuable communications. This work was supported by Research Corporation and the National Science Foundation RUI and MRI programs (Grant Nos. PHY-9721403 and PHY-9724246).

[1] C.S. Wood, S.C. Bennett, D. Cho, B.P. Masterson, J.L. Roberts, C.E. Tanner, and C.E. Wieman, Science **275**, 1759 (1997).
[2] S. A. Blundell, W. R. Johnson, and J. Sapirstein, Phys. Rev. Lett. **65**, 1411 (1990).
[3] Jonathan L. Rosner, Phys. Rev. D **53**, 2724 (1996).
[4] P.A. Vetter, D.M. Meekhof, P.K. Majumder, S.K. Lamoreaux, and E.N. Fortson, Phys. Rev. Lett. **74**, 2658 (1995).
[5] V.A. Dzuba, V.V. Flambaum, P.G. Silvestrov, and O.P. Sushkov, J. Phys. B **20**, 3297 (1987).
[6] V.A. Dzuba, V.V. Flambaum, and M.G. Kozlov, Phys. Rev. A **54**, 3948 (1996); V.V. Flambaum, V.A. Dzuba, and M.G. Kozlov (private communication).
[7] A. Lurio and A.G. Prodell, Phys. Rev. **101**, 79 (1956); P. Gould, *ibid.* **101**, 1828 (1956).
[8] N.H. Edwards, S.J. Phipp, P.E.G. Baird, and S. Nakayama, Phys. Rev. Lett. **74**, 2654 (1995).
[9] P.A. Vetter, Ph.D. dissertation, University of Washington (1995) (unpublished).
[10] A. D. Cronin, E. N. Fortson, S. K. Lamoreaux, and R. B. Warrington, Phys. Rev. Lett. **80**, 3719 (1998).
[11] D.M. Meekhof, P. Vetter, P.K. Majumder, S.K. Lamoreaux, and E.N. Fortson, Phys. Rev. A **52**, 1895 (1995).
[12] Also, magneto-optical effects due to residual *transverse* magnetic fields or field gradients were estimated to be at the negligible 10^{-8} radian level or below.
[13] I.I. Sobel'man, *Introduction to the Theory of Atomic Spectra* (Pergamon Press, New York, 1972).
[14] G.J. Roberts *et al.*, J. Phys. B **13**, 1389 (1980).
[15] C. Chiarella and A. Reichel, Math. Comput. **22**, 137 (1968).
[16] D.V. Neuffer and E.D. Commins, Phys. Rev. A **16**, 844 (1977).
[17] A.M. Martensson-Pendrill (private communication).
[18] N.H. Edwards (private communication).
[19] S.J. Phipp, N.H. Edwards, and P.E.G. Baird, J. Phys. B **29**, 1861 (1996).